Journal of
Materials Chemistry B

Materials for biology and medicine

Accepted Manuscript

This article can be cited before page numbers have been issued, to do this please use: E. Lim, T. A. Vy and S. Lee, *J. Mater. Chem. B*, 2020, DOI: 10.1039/C9TB02494H.

ROYAL SOCIETY OF CHEMISTRY

rsc.li/materials-b

View Article Online
DOI: 10.1039/C9TB02494H

Comparative release kinetics of small drugs (ibuprofen and acetaminophen) from multifunctional mesoporous silica nanoparticles

Eun-Bi Lim, Tran Anh Vy, Sang-Wha Lee*

Department of Chemical and Biological Engineering, Gachon University, 1342 Seongnamdaero, Seongnam-si 13120, Republic of Korea

*E-mail: Lswha@gachon.ac.kr, TEL: +82-31-750-5360

Abstract

Multifunctional mesoporous silica nanoparticles (MSNs) can confer dynamically varied release kinetics depending on the intermolecular interactions between model drugs and functional decorations on MSNs. Herein, brush-like fluorescent conjugates were grafted on the pore walls of pristine MSNs for high drug loading and to impart fluorescence properties. The fluorescent MSNs (FMSNs) were further coated with polydopamine (PDA) and graphene oxide (GO) double layer, so-called FMSNs@PDA and FMSNs@PDA@GO, respectively. The FMSNs@PDA@GO exhibited the highly consistent drug release over one week (~7 days) because of the consolidated PDA/GO double layer at neutral pH 7.4. However, the release rate of FMSN-Ibu@PDA@GO was increased at acidic pH 5.5 because the PDA/GO double layer was partially disrupted due to weakened π-π stacking and electrostatic interactions. The release kinetics of FMSNs-based NPs (FMSNs, FMSNs@PDA, and FMSNs@PDA@GO) was systematically investigated using negatively charged hydrophobic ibuprofen and neutral hydrophilic acetaminophen at pH 7.4. In the FMSN-drug system, the release rate of acetaminophen was higher than that of ibuprofen because of the higher solubility of acetaminophen in aqueous solution. In addition, ibuprofen has the bulky molecular structure as compared to that of acetaminophen, leading to the more retarded transmission through the porous channels of FMSNs. In the FMSNs-drug@PDA system, acetaminophen exhibited a slower release rate than ibuprofen owing to the π-π stacking interaction on the transmission of neutral acetaminophen by the PDA coating layer. On the other hand, FMSNs-drug@PDA@GO exhibited the slower release rate of ibuprofen than acetaminophen, owing to the electrostatic retardation effect by the negative GO layer. Our drug delivery system demonstrated as an

View Article Online
DOI: 10.1039/C9TB02494H

advanced delivery platform of which transmission rate was controlled by intermolecular interactions between the diffusing drugs and functional decorations on the nanocarriers.

Key words: Mesoporous silica, Drug release, Ibuprofen, Acetaminophen, Fluorescent conjugates, Polydopamine, Graphene oxide

1. Introduction

For decades, various therapeutic studies have been conducted on the effects of drug administration on the distribution and delivery of drugs in our bodies. However, drug delivery in the biological matrix experienced the difficulty of reaching to the right place of target area. To solve this problem, various nanocarriers and technologies have been actively developed for efficient and controlled delivery of therapeutic drugs [1, 2]. These nanocarriers include liposomes [3-6], dendrimers [7-9], carbon nanotubes [10, 11], and metal/metal oxide nanoparticles (NPs) [12-16]. Nonetheless, most nanocarriers have certain drawbacks, such as low loading capacity of drugs and early release before reaching the target site [17].

Therefore, mesoporous nanomaterials have emerged as promising nanocarriers with controllable pore sizes, high specific surface areas, high drug-loading capacity, and biocompatibility [18, 19]. In particular, inorganic porous materials (such as MSNs, hydroxyapatites [20], aluminosilicates [21], mesoporous carbons [22], metal organic frameworks [23], and layered silicates) exhibit high chemical and mechanical stability under moderate physiological conditions [24]. Inorganic nanostructures can be tailored to control the rate of diffusion of the adsorbed and encapsulated drugs [25, 26]. Furthermore, they can achieve sustained and controlled release and can act as a diffusion-controlled porous membrane, thus increasing the solubility of poorly soluble drugs or acting as a volume reservoir in drug-eluting devices [27].

Recently, MSNs have been actively employed as smart drug carriers because of their advantages of uniform and adjustable pore size, facile surface modification, and multi-faceted surface synthesis [16]. High drug loading because of its large surface area allows controlled and sustained drug release, which can be achieved by adjusting the pore size and physicochemical nature of the MSNs that influence the transmission of drug molecules [28]. In this aspect, surface modification with biocompatible polydopamine (PDA) can regulate the release of therapeutic drugs and including pH-responsive controlled drug release [29].

View Article Online
DOI: 10.1039/C9TB02494H

Graphene oxide (GO) has a two-dimensional (2D) nanosheet structure with negatively charged functional groups. Thus, GO wrapping improves the colloidal stability of NPs and their capability to target cancer cells [30, 31]. Even though functional decorations of MSNs improve its controlled drug release and specific drug targeting, the structural relationship between physicochemical properties of drugs and the surface characteristics of functional decorations on the nanocarrier has not been systematically investigated.

In this study, MSNs grafted with fluorescent conjugates (FMSNs) were further decorated with polydopamine (PDA) and GO layers, referred to as FMSNs@PDA and FMSNs@PDA@GO, respectively. The release kinetics of FMSNs-based NPs (FMSNs, FMSNs@PDA, and FMSNs@PDA@GO) in phosphate-buffered saline (PBS) solution were systematically investigated with respect to the physicochemical properties of drugs and functional decorations on the FMSNs. In the case of FMSNs-drug system, the release rate of acetaminophen was much higher than ibuprofen because of its higher solubility than ibuprofen. In the case of FMSNs-drug@PDA or FMSNs-drug@PDA@GO system, the drug release rate was strongly influenced by intermolecular interactions (π- π stacking, hydrogen-bonding or electrostatic retardation) with functional decorations on the FMSNs; the PDA layer with aromatic π system delayed the transmission of acetaminophen with resonance structure of π bonding, and the negative GO delayed the transmission of negatively charged ibuprofen at pH 7.4. Notably, FMSNs@PDA@GO exhibited the most consistent and sustained release of the tested drugs over one week (~7 days), suggesting its potential as a promising nanocarrier that can effectively control the dynamic release of small therapeutic agents.

2. Experimental Section

2.1. Chemicals

Tetraethyl orthosilicate (TEOS, 99%), cetyltrimethylammonium bromide (CTAB, 99%), ammonium fluoride (NH_4F, 99.99%), dopamine hydrochloride (DA, powder), GO suspension (2 mg/mL), 3-aminopropyltrimethoxysilane (APTMS, 97%), fluorescein isothiocyanate (FITC, 90%), phosphate-buffered saline (PBS, Bio-ultra, pH 7.4), ibuprofen (Ibu, 98%), and acetaminophen (Acet, 99%) were purchased from Sigma–Aldrich (South Korea). Ethanol and deionized (DI) water (HPLC grade) were used without further purification. All chemicals were used as received. Glassware was cleaned with an acidic solution of HNO_3:HCl (1:3 v/v%) and then rinsed with DI water more than three times.

View Article Online
DOI: 10.1039/C9TB02494H

2.2. Synthesis of fluorescent mesoporous silica nanoparticles (FMSNs)

Fluorescein isothiocyanate (FITC, 2.5 mg) was dissolved in absolute ethanol (3 mL), and an aliquot of APTMS (120 μL) was mixed with the FITC solution. The mixed solution was vigorously stirred at 25 °C for 6 h to form an APTMS-FITC (A-F) complex. All experimental procedures were performed in the dark because of the light sensitivity of the FITC molecule.

MSNs were prepared via a sol-gel technique using TEOS and the cationic surfactant CTAB by the following procedures. CTAB (0.15 g) and NH_4F (0.4 g) were added to 100 mL HPLC water and heated to 80 °C under vigorous stirring (1500 rpm). When the solution color turned into clear, 4.0 mL of TEOS was added dropwise, and the A-F complex solution was gradually added to the sol-gel solution. The color of the mixed solution immediately changed from milky white to yellow. This procedure was carried out in the dark under constant stirring at 80 °C. After 24 h, the yellow solution was centrifuged and washed with DI water and ethanol several times. To remove the CTAB surfactant, the centrifuged precipitates (FMSNs-CTAB) were dispersed in absolute ethanol (150 mL). Next, the solution was vigorously stirred at 80 °C, followed by the slow addition of 2.5 mL 35% hydrochloric acid. This etching process was executed more than two times to remove residual CTAB. Next, the obtained the yellow solid products, i.e., fluorescent MSNs grafted with the A-F complex (so-called FMSNs), were centrifuged, dried in a vacuum oven at 60 °C for 6 h, and stored in the dark before further characterization.

2.3. Drug-loading process

The model drugs used in this study were ibuprofen and acetaminophen. Ibuprofen (Ibu) and acetaminophen (Acet) have been used as analgesics and antipyretics for intermittent and chronic pain conditions [32]. Ibuprofen is a propionic acid derivative with a pKa of 5.2, and acetaminophen is the derivative of acetanilide with a pKa of 9.38 [33, 34]. The solubility of ibuprofen is 0.021 mg/mL and 60 mg/mL at 25 °C in DI water and ethanol, respectively, whereas the solubility of acetaminophen is 14 mg/mL and 25 mg/mL at 25 °C in DI water and ethanol, respectively [35]. In the drug-loading process, FMSNs (100 mg) were dispersed in ethanol (10 mL) solution containing the maximum amount of drugs, e.g., ibuprofen (250 mg) and acetaminophen (600 mg). The mixture was stirred for 24 h in the dark, followed by centrifugation at 12300 rcf (relative centrifugal force) for 15 min to obtain drug-loaded NPs (FMSN-Ibu and FMSN-Acet). The separated NPs were washed several times with DI water to

View Article Online
DOI: 10.1039/C9TB02494H

remove the residual drugs adhered to the surface. Next, the drug-loaded NPs were dried in a vacuum oven at 50 °C for further characterization.

The following experiments were conducted to determine the drug loading amount before and after the surface modifications of MSNs. First, 100 mg of MSNs (or FMSNs) were dispersed for 24 h in an ethanol solution (10 mL) saturated with ibuprofen. After centrifugation of drug-loaded NPs, the absorbance of the remained supernatant was compared with that of the initial ibuprofen solution. The absorbance change of the solution before and after drug loading process is shown in Fig. S1(c, d). Finally, the amounts of ibuprofen loaded in MSNs and FMSNs were calculated using the standard curve of ibuprofen that was obtained at 264 nm, as shown in Fig. S1(a, b). The loading amounts were calculated as 0.4 wt. % and 6.1 wt. % for MSNs-Ibu and FMSNs-Ibu, respectively.

2.4. Polydopamine (PDA) and graphene oxide (GO) coatings

Drug-loaded FMSNs (FMSNs-Drug) were further coated with polydopamine (PDA) and GO double layers to control the release rate of the drug. PDA is an oxidized thin film formed by the self-polymerization reaction of dopamine molecules in weak alkaline conditions [36]. FMSNs-drug (based on 100 mg of FMSNs) and dopamine (10 mg) were mixed in 10 mL of Tris-HCl buffer solution at pH 8.5 and continuously stirred for 3 h at RT. After completing the PDA coating process, the final product was centrifuged at 12300 rcf for 10 min, washed several times with DI water, and dried in a vacuum oven at 60 °C for 6 h. Lastly, Added 1.0 mL of GO suspension (2 mg/mL in water) in the solution in which MSNs-Drug@PDA (1.0 g) is dispersed. The mixed solution was stirred for 4 h in the dark. Next, the sample was centrifuged (at 12300 rcf for 10 min) and washed with DI water several times to remove the residual GO. The final product was dried in a vacuum oven at 60 °C for 6 h and kept in a desiccator. Additionally, Acet is highly soluble in aqueous solution, so Acet easily escapes from the FMSNs during the PDA coating process. Thus, FMSNs-Acet was PDA coated in a saturated solution of acetaminophen (adds Acet to Tris-HCl buffer), in contrast with PDA coating on Ibu-loaded FMSNs.

2.5. Characterization of materials

The nitrogen adsorption and desorption isotherms measurement of MSNs and FMSNs were obtained from specific surface area analyzer (ASAP2020) from Micromeritics. Their specific surface area and pore distribution were calculated using Brunauer–Emmett–Teller

View Article Online
DOI: 10.1039/C9TB02494H

(BET) and Barrett-Joyner-Halenda (BJH) analysis theory, respectively. Scanning electron microscope (SEM) images were taken on a S-4700, MONO CL (Hitachi) and transmission electron microscope (TEM) images were taken on a H7600 (Hitachi) at an accelerating voltage of 80kV. Fluorescence Spectroscopy System (FL, FRET MASTER-1, P.T.I) was used to characterize the Fluorescence of the samples under excitation wavelength of 470 nm. The functional groups of the prepared samples were characterized by Fourier transform infrared spectroscopy (FTIR, Vertex 70, Bruker) in the range of 4500 to 500 cm^{-1}.

2.6. In-vitro release test

The as-prepared samples (FMSNs-Drug, FMSNs-Drug@PDA, FMSNs-Drug@PDA@GO) were suspended in 10 mL of PBS (pH 7.4) under constant stirring at 37 ± 0.5 °C. The drug release begun immediately after the sample was added to the PBS solution. To determine the released amounts of drug, a standard curve in aqueous solution was obtained over a concentration range (Fig. S2 and S3) showing the linear behavior of Beer–Lambert′s law. The measurement of drug release was periodically taken an aliquot from the in-vitro solution and the change in absorbances were measured using a nanodrop absorption analyzer (nano drop 2000, Thermo Fisher Scientific Inc.). In the case of PDA/GO-coated samples (FMSNs-Drug@PDA, FMSNs-Durg@PDA@GO), approximately 0.3 mL aliquots were taken in a 1.5 mL micro-tube and centrifuged to remove any disturbing impurities for the correct measurement of supernatant absorbance. To investigate the effect of pH on the release rate, in-vitro release tests were also performed at pH 5.5 and pH 7.4 using the GO/PDA-coated FMSNs (FMSNs-Drug@PDA@GO) sample. The changes in absorbance of the solution were measured at 222 and 243 nm for detecting Ibu and Acet, respectively.

$$Releasing\ amounts\ (\%) = \frac{\text{Amount of released drug in medium}}{\text{Amount of loaded drug in NPs}} \times 100\% \qquad (1)$$

3. Result and discussion

3.1. Synthesis and characterization of the as-prepared samples

According to **Scheme 1,** the modified sol-gel method produces uniform spherical silica NPs [37], in which the cationic surfactant CTAB forms micelles embedded in the silica matrix via hydrolysis and condensation of TEOS. Next, APTMS-FITC (A-F) complex was grafted on the porous channels of MSNs, which were formed by removing CTAB micelles with HCl (35 wt. %)

View Article Online
DOI: 10.1039/C9TB02494H

treatment. The A-F complex was covalently linked with the surface hydroxyl groups of MSNs, forming fluorescent MSNs (FMSNs). After drug loading, the FMSNs were further coated with a PDA and GO double layer to control the release of drugs.

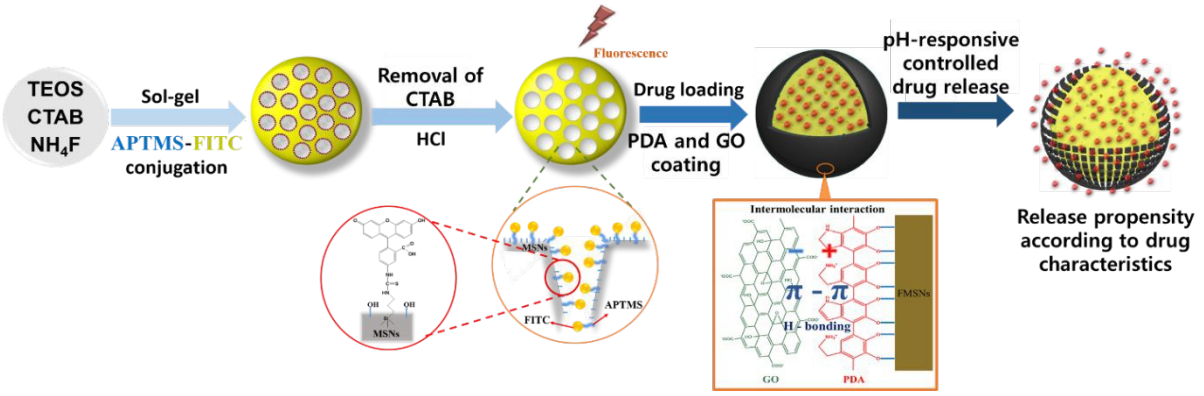

Scheme 1. Schematic snapshots illustrating the fabrication process of MSNs grafted with APTMS-FITC conjugates, followed by coating of the PDA and GO double layer, and their controlled drug release mechanism.

BET analysis. The N_2 adsorption/desorption isotherms of mesoporous NPs and their pore size distribution by BJH analysis are shown in **Fig. 1**. The obtained adsorption/desorption isotherms are close to type IV isotherms [38]. At the initial part of the adsorption isotherm, the adsorption capacity sharply increased, which was indicative of the presence of abundant micropores. In reference, FMSNs was prepared by grafting A-F complex on the pore walls of MSNs. At the beginning of the isotherm, the adsorption slope of FMSNs sample is steeper than that of MSN sample. In addition, FMSNs sample exhibited the rapid capillary condensation phenomenon before reaching to the saturation pressure, indicating the rich formation of micropores in FMSNs [39]. After the MSNs were grafted with fluorescent A-F complex, the BET surface area of the FMSNs significantly increased from 209 m^2/g to 3391 m^2/g. The pore volume and pore size also increased from 0.46 cm^3/g to 4.00 cm^3/g and 2.5 nm to 3.0 nm, respectively. A significant increase in the surface area was mainly attributed to the development of numerous micropores and large mesopores, probably due to the grafting of A-F complex on the pore walls during sol-gel process. The increased surface area is also beneficial for enhancing the loading capacity of testing drugs [40]. Table S1 summarizes the BET-BJT results of the MSN and FMSN samples. As evidence for the BET results, the loading amounts of ibuprofen in MSNs and FMSNs (100 mg) were compared, as shown in the experimental section. The loading amounts of ibuprofen were approximately 0.4 wt. % and 6.1 wt. % for MSNs and FMSNs, respectively. The significant difference (15 times) in the loading

View Article Online
DOI: 10.1039/C9TB02494H

capacity agreed with the considerable difference in surface areas (16 times) between MSNs and FMSNs.

SEM and TEM analysis. The as-synthesized samples were characterized by SEM and TEM, and the results are shown in **Fig. 2**. The SEM images of MSNs showed a spherical morphology with a uniform size distribution (**Fig. 2a**). As compared with the pristine MSNs, FMSNs exhibited a three-dimensional assembly of NPs with a somewhat roughened surface morphology (**Fig. 2b**). After the FMSNs were coated with a PDA layer (FMSNs@PDA), the shape of the FMSNs@PDA slightly deviated from the spherical shape with a more roughened surface morphology (**Fig. 2c**). The thickness of the PDA layer was estimated as ~3–4 nm. **Fig. 2d** shows the TEM images of complete GO wrapping over NPs, i.e., the GO-coated FMSNs@PDA (FMSNs@PDA@GO). In general, GO wrapping increased the colloidal stability of the NPs and resulted in more consistent drug release. [41] According to dynamic light scattering (DLS) analysis, the NPs exhibited an increasing particle size according to the additional decorations of PDA and GO layers: FMSNs < FMSNs@PDA < FMSNs@PDA@GO (Table S1).

PL measurements. Fluorescence properties of the as-prepared samples (MSNs, FMSNs, FMSNs@PDA, and FMSNs@PDA@GO) are illustrated in **Fig. 3**. All samples showed fluorescence spectra with an emission peak at 517 nm under excitation of λ_{ex} = 470 nm, except for the pristine MSNs without any fluorescence. The FMSNs@PDA and FMSNs@PDA@GO showed relatively low fluorescence intensity because some fraction of the fluorescence emission was blocked or quenched by PDA and GO coating layers. Thus, the comparative FL intensity confirmed that the fluorescent conjugates, PDA, and GO layers were successfully functionalized. The FMSNs-based NPs can act as bio-imaging agents that can localize in the transport pathway and at targeted locations during the course of drug delivery.

FT-IR analysis. FT-IR analysis was performed to verify the successful functionalization of the as-prepared samples. **Fig. 4a** shows the FT-IR spectra of pristine MSNs, showing infrared (IR) bands attributed to the asymmetric vibration of Si–O (1070 cm^{-1}) and Si–OH (850 cm^{-1}) and to the symmetric vibration of Si–O (795 cm^{-1}). The IR bands between 700 and 1280 cm^{-1} can be ascribed to the superimpositions of SiO_2 peaks, Si–OH bonding, and various peaks of residual organic groups. Water shows a weak and broad band between 3300 cm^{-1} and 3600 cm^{-1}, which can be assigned to O–H stretching of adsorbed water. After grafting with A-F complex, the resulting FMSNs exhibited new bands at 1395 cm^{-1} and 1680 cm^{-1}, which were assigned to C=S and C–O vibrations. Furthermore, the broad absorption band at 3300 to 3500

View Article Online
DOI: 10.1039/C9TB02494H

cm^{-1} was assigned to the N–H stretching vibration. (**Fig. 4b**). PDA-coated FMSNs (FMSNs@PDA) showed broad bands indicating O–H and N–H stretching at 3285 cm^{-1}. Additional bands at 1751, 1634, and 1480 cm^{-1} were attributed to the C=O, C=C, and C–N bonds in the benzene ring, respectively (**Fig. 4c**). GO-wrapped FMSNs@PDA (FMSNs@PDA@GO) showed amplified bands at 1670 and 1296 cm^{-1}, corresponding to the carbonyl C=O bond associated with the aromatic vibration of the unoxidized graphite domain and C–O stretch associated with a carboxylic acid. Also, the characteristic bands at 3439 and 2925 cm^{-1} were assigned to O–H groups and C–H groups, respectively **(Fig. 4d**). All FT-IR spectra demonstrated successful functionalization during the consecutive synthetic steps of FMSN-based NPs.

3.2. In-vitro drug release test

3.2.1. Kinetic models of drug diffusion

Based on the initial loading and total release amounts, the cumulative release of the sample usually did not show the complete release of the originally loaded amounts. This observation could be caused by several possible reasons: i) some fraction of the initial loading was lost during surface modification of drug-loaded MSNs; ii) a small fraction of loaded drug was retained in the deep pores of the samples even after prolonged release times. In addition, some fraction of loaded drug was released immediately after in-vitro release test because of its surface adherence to the sample. All these factors make it difficult to interpret the release kinetics of drugs loaded in the MSNs. To account for all deviating factors for release kinetics, we suggested the following equation based on the normalized fraction of the released drug in the solution [42].

$$\frac{F_t}{F_\infty} = \frac{Q_t - Q_o}{Q_\infty - Q_o}; \begin{cases} at\ t = 0,\ \frac{F_t}{F_\infty} = 0 \\ at\ t = \infty,\ \frac{F_\infty}{F_\infty} = 1 \end{cases} \qquad (2)$$

where Q_0 is the initial amount of drug in the solution or the amount of drug immediately released because of surface attachment at t = 0+; Q_∞ is the final amount of drug in the solution at $t = \infty$, and Q_t is the amount of drug in the solution at time t. Thus, F_t/F_∞ is the normalized fraction of the released drug at equilibrium time ($t = \infty$) versus at zero time (t = 0+).

View Article Online
DOI: 10.1039/C9TB02494H

Three types of mathematical models can describe the release kinetics of the drug delivery system. First, drug release can be interpreted as an exponential type of diffusion based on the Noyes-Whitney equation and Fick's law:

$$\frac{F_t}{F_\infty} = 1 - e^{-k_F t} \quad (3)$$

where F_t/F_∞ is the normalized fraction of the released drug from t = 0+ to t = ∞. k_F is the first-order rate constant independent of drug concentration, which includes information on solvent accessibility to the substrate and the diffusion coefficient through the mesoporous matrix [43, 44].

The release kinetics were also analyzed by a power-law equation based on the Korsmeyer–Peppas (K–P) model, which is usually employed to describe the anomalous diffusion of drug release:

$$\frac{F_t}{F_\infty} = k_R t^n \quad (4)$$

where F_t/F_∞ is the normalized fraction of drug released at time t, k_R is the first-order relaxation constant incorporating the structural and geometric properties of the drug delivery system, and n is a release exponent. In the K–P model, the value of n characterizes the release mechanism [43, 44]. For the sphere matrix, n = 0.43 indicates Fickian diffusion, $0.43 < n < 0.85$ corresponds to anomalous diffusion, and $n \geq 0.85$ corresponds to relaxation-controlled diffusions [43, 45].

The square-root-of-time dependence of the release kinetics can be predicted by a simplified Higuchi model [43, 46]:

$$\frac{F_t}{F_\infty} = k_H t^{1/2} \quad (5)$$

where F_t/F_∞ is the normalized cumulative fraction of drug released at time t, K_H is the Higuchi release constant reflecting the design variables of the system [47, 48]. This model is useful for studying the release of water-soluble and poorly soluble drugs from a variety of matrices including porous solids.

View Article Online
DOI: 10.1039/C9TB02494H

3.2.2. Drug release kinetics of FMSNs-drug systems

As described in the experimental section, the amount of released drugs was measured periodically to monitor the release kinetics of FMSN-drug systems. In reference, the carboxylic acid group of ibuprofen with alkyl branches is not included in the resonance structure of benzene. On the other hand, acetaminophen has a two-dimensional (2-D) flat structure to ensure the conjugation of π bonds throughout the molecule. **Fig. 5a and 5b** shows the release behavior of small drugs (ibuprofen and acetaminophen) from FMSN-based nanocarriers in PBS, respectively. The release rate profiles of both drugs showed the following order – FMSNs-drug > FMSNs-drug@PDA > FMSNs-drug@PDA@GO, probably due to intermolecular interactions (π-π stacking, hydrogen bonding or electrostatic retardation) between the testing drugs and functional decorations on the FMSNs.

According to **Fig. 5(a1-a3, b1-b3)**, the release characteristics of ibuprofen (Ibu) and acetaminophen (Acet) were different from each other depending on the types of drug molecules and functional decorations. As previously mentioned, ibuprofen has hydrophobic alkyl branches so that its solubility in PBS is quite limited. On the other hand, acetaminophen has a high solubility in PBS because of the presence of hydrophilic groups such as hydroxyl, carboxyl, and amide groups. According to the release kinetics of FMSN-drug systems shown in **Fig. 5a-1** and **b-1**, the cumulative release fraction was 90% at 36 h for Ibu and 15 h for Acet, respectively. The release rate of FMSNs-Ibu was distinctly lower than that of FMSNs-Acet because of the higher solubility of Acet than Ibu in PBS. The fast release kinetics of the FMSN-drug systems was predicted by Fickian equation, and the fitted values of k_F were 0.38 and 0.62 for Ibu and Acet, respectively. Based on the k_F values fitted for both systems, Acet exhibited a 40% higher release rate (based on the release fraction of 90%) than Ibu. Notably, MSN-Ibu (k_F = 0.5) exhibited a 30% higher release rate than FMSNs-Ibu (k_F = 0.38), (Fig. S4). The distinct retardation effect by brush-like conjugates grafted on porous channels was observed for the transmission of ibuprofen with the bulky structure rather than acetaminophen with the flat structure.

In contrast to the distinct differences in release rates between FMSNs-Ibu and FMSNs-Acet systems, no significant differences of release kinetics were observed between FMSNs-Ibu@PDA and FMSNs-Acet@PDA systems. This result indicates that the PDA coating provided an effective blocking layer for the rapid transmission of acetaminophen. As shown in **Fig. 5a-2** and **b-2**, the K-P model was applied to the first 60% of the fractional release data and

View Article Online
DOI: 10.1039/C9TB02494H

the fitted values were n = 0.47 and k_R = 19.61 for FMSNs-Ibu@PDA and n = 0.62 and k_R = 15.0 for FMSNs-Acet@PDA [49]. According to the analysis using the K–P model, the FMSNs-Acet@PDA exhibited highly anomalous diffusion behavior because the relation exponent of n = 0.62 was higher than the Fickian value of n = 0.43. **Fig. S5** shows the application of the Higuchi model to the release data of FMSN-drug@PDA in spite of deviation of release data from the Higuchi model. The Higuchi constants were fitted as k_H = 32.96 and k_H = 31.26 for FMSNs-Ibu@PDA and FMSNs-Acet@PDA, respectively. FMSNs-Ibu@PDA showed a similar (or a slightly higher) release rate when compared with that of FMSNs-Acet@PDA, in contrast with the opposite trends observed for the FMSNs-drug system.

This result clearly indicates that PDA coating provided the effective retardation barrier for the transmission of acetaminophen, probably due to its π-π stacking interactions with PDA coating layer [50]. Acetaminophen has the 2-D resonance structure with π bonding, and its planar structure can maximize the π-π interactions with the PDA layer consisting of aromatic π system. In contrast, ibuprofen has the 3-D molecular structure and has the narrow delocalization of π electrons, resulting in relatively unobstructed transmission of ibuprofen. Thus, the π-π stacking interaction played as the main factor for the retarded transmission of acetaminophen through the PDA layer.

The slow release kinetics of FMSNs-drug@PDA@GO was well fitted using the Higuchi model. As seen from **Fig. 5a-3** and **b-3**, the release rate of MSNs-drug@PDA@GO agreed well with the square-root-of-time dependence that was expected by the Higuchi model. In particular, the FMSN-Ibu@PDA@GO showed the first Higuchi line (k_H = 23.62) up to the release fraction of ~70%, followed by the second Higuchi line (k_H = 8.87) up to ~95%. In contrast, the FMSNs-Acet@PDA@GO exhibited one Higuchi line (k_H = 25.40) up to the release fraction of ~95%. Overall, the PDA/GO double layer was found to be considered effective for the consistent and sustained release of small drugs. In the case of the FMSNs-drug@PDA@GO system, Ibu exhibited the slower release rate than that of Acet.

For the PDA/GO double layer coating, however, the release kinetics of FMSNs-drug@PDA@GO was influenced by the combined interactions (π-π stacking, hydrogen bonding or electrostatic retardation). For instance, ibuprofen exhibited the slower release rate than that of acetaminophen. At neutral pH 7.4, acetaminophen and PDA is neutral, but ibuprofen and GO are negatively charged. Thus, the transmission of negative ibuprofen can be electrostatically retarded by the presence of negative GO barrier. On the other hand, the transmission of neutral acetaminophen was not significantly influenced by the negative GO

View Article Online
DOI: 10.1039/C9TB02494H

layer. All the fitted parameter values using the three different models are summarized in Table S2.

The effects of pH on the release kinetics are shown in **Fig. 6**. The release kinetics of FMSNs-Ibu@PDA@GO in PBS solution were compared at acidic pH 5.5 and neutral pH 7.4. According to **Fig. 6a**, the FMSNs-Ibu@PDA@GO system showed the higher release rate at pH 5.5 than that at pH 7.4. The difference in release rates between pH 5.5 and pH 7.4 was about 13–17% during the release time from 10 h to 70 h. As shown in **Fig. 6b**, the Higuchi model was applied to fit release kinetics of the FMSNs-Ibu@PDA@GO system, and the fitted k_H value was 32.04 at pH 5.5, which is much higher than $k_H = 23.62$ at pH 7.4. The faster release rate of ibuprofen at pH 5.5 was attributed to the partial disruption of π–π stacking and/or electrostatic interactions between the PDA and GO layers. At acidic pH condition, the increase in the ratio of deprotonated to protonated carboxylic acid groups in GO nanosheets leads to the less hydrophilic self-agglomeration state of GO which is easily detached from the PDA coating layer [51, 52]. Another reason may be that the loosened PDA/GO double layer can lead to the increased release rate of ibuprofen at pH 5.5. If the molecular structure of PDA is not completely cyclized, a few amine groups are positively charged on the PDA layer at neutral pH 7.4. Thus, the electrostatic interactions between the PDA and GO layers may be weakened at acidic pH 5.5.

To elucidate the transmission mechanism by intermolecular interactions more clearly, the pH effect on the transmission acetaminophen was investigated using the FMSNs-drug@PDA@GO system. According to Fig. S6, the release rate of acetaminophen was not significantly influenced by the pH changes (from pH 7.4 to pH 5.5), showing the slight increase of release rate at pH 5.5 after 20 h. This result indicates that acetaminophen is more strongly influenced by the π-π interactions with the PDA layer rather than by the disruption of PDA/GO double layer. The slight increase of release fraction at 20–40 h was probably due to the PDA layer loosened from the FMSNs at acidic pH 5.5 [29]. To be conclusive, the release rate of neutral acetaminophen was mainly influenced by the π- π stacking interactions with the PDA layer, irrespective of pH changes. On the other hand, the release rate of negative ibuprofen was significantly influenced by the pH changes. The increased release rate of ibuprofen at acidic pH is mainly attributed to the loss of electrostatic interactions and/or disrupted π-π interactions between the PDA and GO layers, leading to the faster transmission of ibuprofen.

In summary, acetaminophen is a hydrophilic drug with a planar 2-D structure, whereas ibuprofen is a hydrophobic drug with a bulky 3-D structure. As a result, acetaminophen tends

View Article Online
DOI: 10.1039/C9TB02494H

to be released faster than ibuprofen in the FMSNs-drug system. In the case of FMSNs-drug@PDA system, there was no significant difference of release kinetics between ibuprofen and acetaminophen, indicating that the π-π stacking interaction is the main factor for the retarded transmission of acetaminophen through the PDA layer. In the case of FMSNs-drug@PDA@GO system, ibuprofen exhibited the slower release rate than that of acetaminophen. At neutral pH 7.4, the transmission of negative ibuprofen was electrostatically retarded by the presence of negative GO barrier, but the transmission of ibuprofen was significantly increased due to the partials disruption of PDA/GO double layer at acidic pH 5.5.

4. Conclusions

In this work, pristine MSNs were grafted with fluorescent A-F complex, and the resulting FMSNs were subsequently coated with PDA and GO layers, which were referred to as FMSNs@PDA and FMSNs@PDA@GO. These nanocarriers were suitable for fluorescent imaging, high drug loading, and controlled drug release because of the formation of consolidated PDA/GO double layer. The drug release kinetics was investigated by focusing on the physicochemical interactions between the testing drugs and functional decorations on the FMSNs. The rapid release kinetics of FMSNs-drug system was predicted by the Fickian exponential equation, and the slow release kinetics of FMSNs-drug@PDA@GO system was predicted by the Higuchi model. The intermediate release kinetics of FMSNs-drug@PDA system was predicted by the K–P model. In the case of FMSNs-drug system, the release rate of acetaminophen was faster than that of ibuprofen because of its higher solubility. After the FMSNs were coated with PDA and GO layers, the release rates of small drugs were significantly influenced by intermolecular interactions (π-π stacking, hydrogen-bonding or electrostatic retardation) between the testing drugs and functional decorations on the FMSNs. In the case of FMSNs-Ibu@PDA@GO, the transmission of ibuprofen was significantly increased due to the partials disruption of PDA/GO double layer at acidic pH 5.5. Our drug delivery system suggested as a potential delivery platform of which transmission rate was controlled by intermolecular interactions between the diffusing drugs and functional decorations on the nanocarriers.

Acknowledgments.

This work was supported by the National Research Foundation of Korea (NRF-2016R1D1A1B03931486). This work was also supported by the Korea Institute of Energy

View Article Online
DOI: 10.1039/C9TB02494H

Technology Evaluation and Planning (KETEP), the Ministry of Trade, Industry & Energy (MOTIE) of the Republic of Korea [20174030201530]. We thank the Smart Materials Research Center for IoT at Gachon University for its instrumental support.

References

1. Li, C., et al., *Recent progress in drug delivery.* Acta Pharmaceutica Sinica B, 2019.
2. Yun, Y.H., B.K. Lee, and K. Park, *Controlled Drug Delivery: Historical perspective for the next generation.* J Control Release, 2015. **219**: p. 2-7.
3. M. Çağdaş, A.D.S., S. Bucak, *Liposomes as Potential Drug Carrier Systems for Drug Delivery.* Appl. Nanotech. Drug Delivery, 2014: p. pp. 1-51.
4. Allen, T.M. and P.R. Cullis, *Liposomal drug delivery systems: from concept to clinical applications.* Adv Drug Deliv Rev, 2013. **65**(1): p. 36-48.
5. Barani, H. and M. Montazer, *A review on applications of liposomes in textile processing.* J Liposome Res, 2008. **18**(3): p. 249-62.
6. Pattni, B.S., V.V. Chupin, and V.P. Torchilin, *New Developments in Liposomal Drug Delivery.* Chemical Reviews, 2015. **115**(19): p. 10938-10966.
7. Kaminskas, L.M., et al., *Association of chemotherapeutic drugs with dendrimer nanocarriers: an assessment of the merits of covalent conjugation compared to noncovalent encapsulation.* Mol Pharm, 2012. **9**(3): p. 355-73.
8. D'Emanuele, A. and D. Attwood, *Dendrimer-drug interactions.* Adv Drug Deliv Rev, 2005. **57**(15): p. 2147-62.
9. Liu, M. and J.M.J. Fréchet, *Designing dendrimers for drug delivery.* Pharmaceutical Science & Technology Today, 1999. **2**(10): p. 393-401.
10. Yamashita, T., et al., *Carbon Nanomaterials: Efficacy and Safety for Nanomedicine.* Materials (Basel), 2012. **5**(2): p. 350-363.
11. Liu, Z., et al., *Carbon materials for drug delivery & cancer therapy.* Materials Today, 2011. **14**(7-8): p. 316-323.
12. Ghosh, P., et al., *Gold nanoparticles in delivery applications.* Adv Drug Deliv Rev, 2008. **60**(11): p. 1307-15.
13. Arruebo, M., et al., *Magnetic nanoparticles for drug delivery.* Nano Today, 2007. **2**(3): p. 22-32.
14. Trouiller, B., et al., *Titanium dioxide nanoparticles induce DNA damage and genetic instability in vivo in mice.* Cancer Res, 2009. **69**(22): p. 8784-9.
15. Wang, S., *Ordered mesoporous materials for drug delivery.* Microporous and Mesoporous Materials, 2009. **117**(1-2): p. 1-9.
16. Narayan, R., et al., *Mesoporous Silica Nanoparticles: A Comprehensive Review on Synthesis and Recent Advances.* Pharmaceutics, 2018. **10**(3).
17. Tran, V.A. and S.W. Lee, *A prominent anchoring effect on the kinetic control of drug*

View Article Online
DOI: 10.1039/C9TB02494H

release from mesoporous silica nanoparticles (MSNs). J Colloid Interface Sci, 2018. **510**: p. 345-356.

18. Arruebo, M., *Drug delivery from structured porous inorganic materials.* Wiley Interdiscip Rev Nanomed Nanobiotechnol, 2012. **4**(1): p. 16-30.
19. Vallet-Regi, M., F. Balas, and D. Arcos, *Mesoporous materials for drug delivery.* Angew Chem Int Ed Engl, 2007. **46**(40): p. 7548-58.
20. Zhang, C., et al., *Self-activated luminescent and mesoporous strontium hydroxyapatite nanorods for drug delivery.* Biomaterials, 2010. **31**(12): p. 3374-83.
21. Byrne, R.S. and P.B. Deasy, *Use of porous aluminosilicate pellets for drug delivery.* J Microencapsul, 2005. **22**(4): p. 423-37.
22. Saha, D., K.E. Warren, and A.K. Naskar, *Soft-templated mesoporous carbons as potential materials for oral drug delivery.* Carbon, 2014. **71**: p. 47-57.
23. Huxford, R.C., J. Della Rocca, and W. Lin, *Metal-organic frameworks as potential drug carriers.* Curr Opin Chem Biol, 2010. **14**(2): p. 262-8.
24. Zhang, L., et al., *Nanoparticles in medicine: therapeutic applications and developments.* Clin Pharmacol Ther, 2008. **83**(5): p. 761-9.
25. Hartmann, M., *Ordered Mesoporous Materials for Bioadsorption and Biocatalysis.* Chemistry of Materials, 2005. **17**(18): p. 4577-4593.
26. Wang, Y., A.D. Price, and F. Caruso, *Nanoporous colloids: building blocks for a new generation of structured materials.* Journal of Materials Chemistry, 2009. **19**(36).
27. Rigby, S.P., M. Fairhead, and C.F. van der Walle, *Engineering silica particles as oral drug delivery vehicles.* Current Pharmaceutical Design, 2008. **14**(18): p. 1821-1831.
28. Nieto, A., et al., *Surface electrochemistry of mesoporous silicas as a key factor in the design of tailored delivery devices.* Langmuir, 2010. **26**(7): p. 5038-49.
29. Zheng, Q., et al., *Mussel-inspired polydopamine coated mesoporous silica nanoparticles as pH-sensitive nanocarriers for controlled release.* Int J Pharm, 2014. **463**(1): p. 22-6.
30. Chowdhury, I., et al., *Colloidal properties and stability of graphene oxide nanomaterials in the aquatic environment.* Environ Sci Technol, 2013. **47**(12): p. 6288-96.
31. Tran, A.V., et al., *Targeted and controlled drug delivery by multifunctional mesoporous silica nanoparticles with internal fluorescent conjugates and external polydopamine and graphene oxide layers.* Acta Biomater, 2018. **74**: p. 397-413.
32. Moore, R.A., et al., *Overview review: Comparative efficacy of oral ibuprofen and paracetamol (acetaminophen) across acute and chronic pain conditions.* Eur J Pain, 2015. **19**(9): p. 1213-23.
33. Dastmalchi, S., M. Rashidi, and M. Rassi, *Simultaneous determination of the pKa and octanol/water partition coefficient (Pm) of acetaminophen.* J J Sch Pharm Med Sci Univ Tehran, 1995. **4**: p. 7-14.
34. Herzfeld CD and K. R., *Dissociation constant, solubilities and dissolution rate of some selective non steroidal anti inflammatory drugs.* Drug Dev Ind Pharm, 1983. **9**(5): p. 767-

View Article Online
DOI: 10.1039/C9TB02494H

793.

35. Yalkowsky, S.H. and R.M. Dannenfelser, *Aquasol database of aqueous solubility.* College of Pharmacy, University of Arizona, Tucson, 1992. **189**(AZ).
36. Ryu, J.H., P.B. Messersmith, and H. Lee, *Polydopamine Surface Chemistry: A Decade of Discovery.* ACS Appl Mater Interfaces, 2018. **10**(9): p. 7523-7540.
37. Trewyn, B.G., et al., *Synthesis and functionalization of a mesoporous silica nanoparticle based on the sol-gel process and applications in controlled release.* Acc Chem Res, 2007. **40**(9): p. 846-53.
38. Sing, K.S.W., *Reporting physisorption data for gas/solid systems with special reference to the determination of surface area and porosity (Recommendations 1984).* Pure and Applied Chemistry, 1985. **57**(4): p. 603-619.
39. Rasmussen, C.J., et al., *Cavitation in metastable liquid nitrogen confined to nanoscale pores.* Langmuir, 2010. **26**(12): p. 10147-57.
40. Muñoz, B., et al., *MCM-41 Organic Modification as Drug Delivery Rate Regulator.* Chemistry of Materials, 2003. **15**(2): p. 500-503.
41. Devanathan, R., et al., *Molecular Dynamics Simulations Reveal that Water Diffusion between Graphene Oxide Layers is Slow.* Scientific Reports, 2016. **6**: p. 29484.
42. Manzano, M., et al., *Studies on MCM-41 mesoporous silica for drug delivery: Effect of particle morphology and amine functionalization.* Chemical Engineering Journal, 2008. **137**(1): p. 30-37.
43. Costa, P. and J.M. Sousa Lobo, *Modeling and comparison of dissolution profiles.* European Journal of Pharmaceutical Sciences, 2001. **13**(2): p. 123-133.
44. Izquierdo-Barba, I., et al., *Influence of mesoporous structure type on the controlled delivery of drugs: release of ibuprofen from MCM-48, SBA-15 and functionalized SBA-15.* 2009. **50**(3): p. 421-429.
45. Peppas, N.A. and J.J. Sahlin, *A simple equation for the description of solute release. III. Coupling of diffusion and relaxation.* International Journal of Pharmaceutics, 1989. **57**(2): p. 169-172.
46. Higuchi, T., *Mechanism of sustained-action medication. Theoretical analysis of rate of release of solid drugs dispersed in solid matrices.* Journal of Pharmaceutical Sciences, 1963. **52**(12): p. 1145-1149.
47. Siepmann, J. and N.A. Peppas, *Higuchi equation: derivation, applications, use and misuse.* Int J Pharm, 2011. **418**(1): p. 6-12.
48. Paul, D.R., *Elaborations on the Higuchi model for drug delivery.* Int J Pharm, 2011. **418**(1): p. 13-7.
49. Dash, S., et al., *Kinetic Modeling on Drug Release from Controlled Drug Delivery Systems.* Acta Poloniae Pharmaceutica, 2010. **67**(3): p. 217-223.
50. Zheng, X., et al., *Polydopamine Coatings in Confined Nanopore Space: Toward Improved Retention and Release of Hydrophilic Cargo.* The Journal of Physical Chemistry C, 2015.

View Article Online
DOI: 10.1039/C9TB02494H

119(43): p. 24512-24521.

51. May-Masnou, A., et al., *Solubilization of decane into gemini surfactant with a modified Jeffamine backbone: Design of hierarchical porous silica.* Microporous and Mesoporous Materials, 2013. **169**: p. 235-241.
52. He, D., et al., *Remote-controlled drug release from graphene oxide-capped mesoporous silica to cancer cells by photoinduced pH-jump activation.* Langmuir, 2014. **30**(24): p. 7182-9.

View Article Online
DOI: 10.1039/C9TB02494H

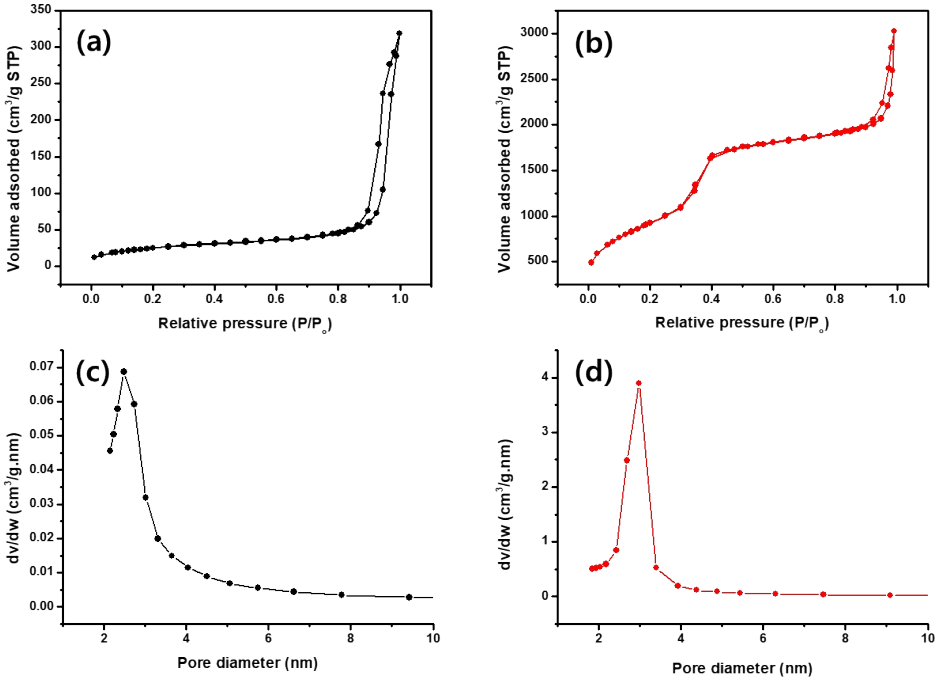

Fig. 1. Nitrogen adsorption/desorption isotherms of (a) MSNs and (b) FMSNs, and pore size distribution of (c) MSNs and (d) FMSNs.

View Article Online
DOI: 10.1039/C9TB02494H

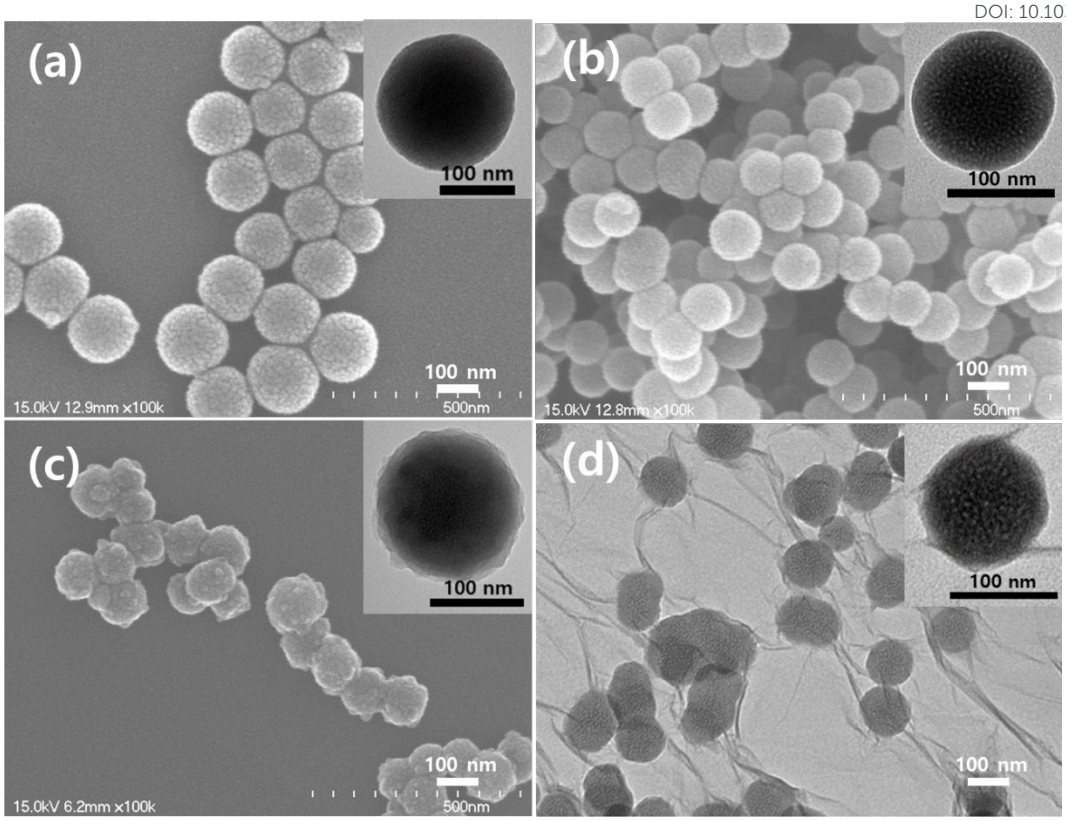

Fig. 2. SEM and TEM (inset) images of (a) MSNs, (b) FMSNs, and (c) FMSNs@PDA and TEM images of (d) FMSNs@PDA@GO.

View Article Online
DOI: 10.1039/C9TB02494H

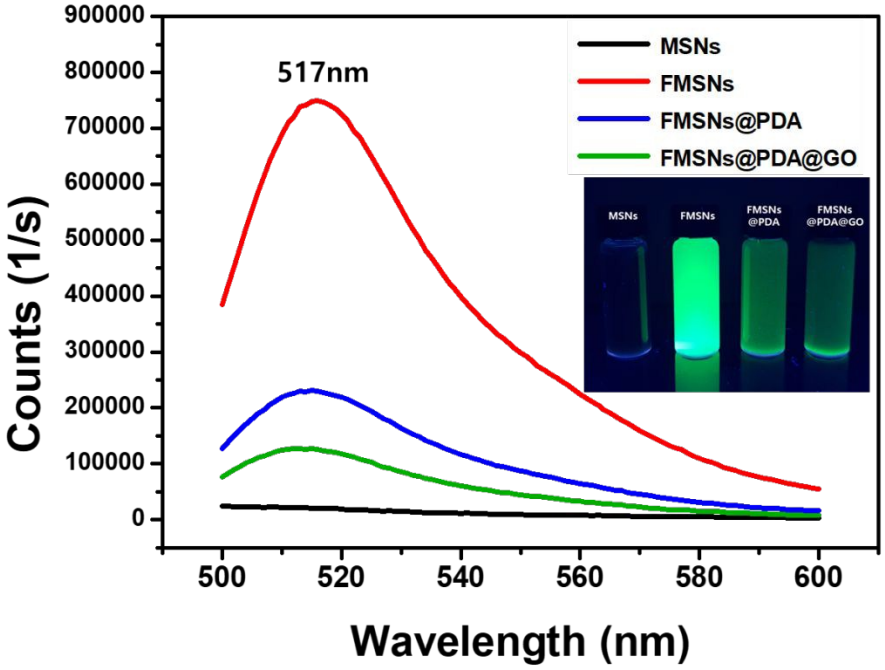

Fig. 3. Photoluminescence (PL) emission spectra of MSNs, FMSNs, FMSNs@PDA, and FMSNs@PDA@GO. The inset shows UV-irradiated fluorescence visibility obtained from MSNs, FMSNs, FMSNs@PDA, and FMSNs@PDA@GO solutions.

View Article Online
DOI: 10.1039/C9TB02494H

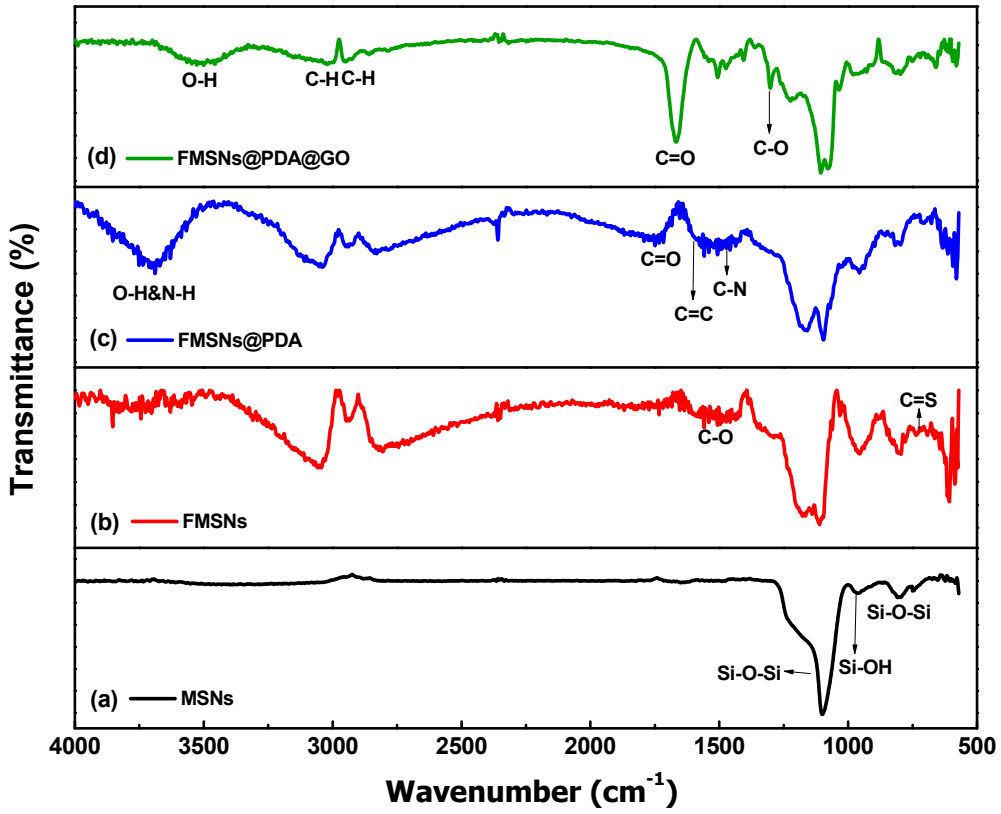

Fig. 4. FT-IR spectra of (a) MSNs, (b) FMSNs, (c) FMSNs@PDA, and (d) FMSNs@PDA@GO.

View Article Online
DOI: 10.1039/C9TB02494H

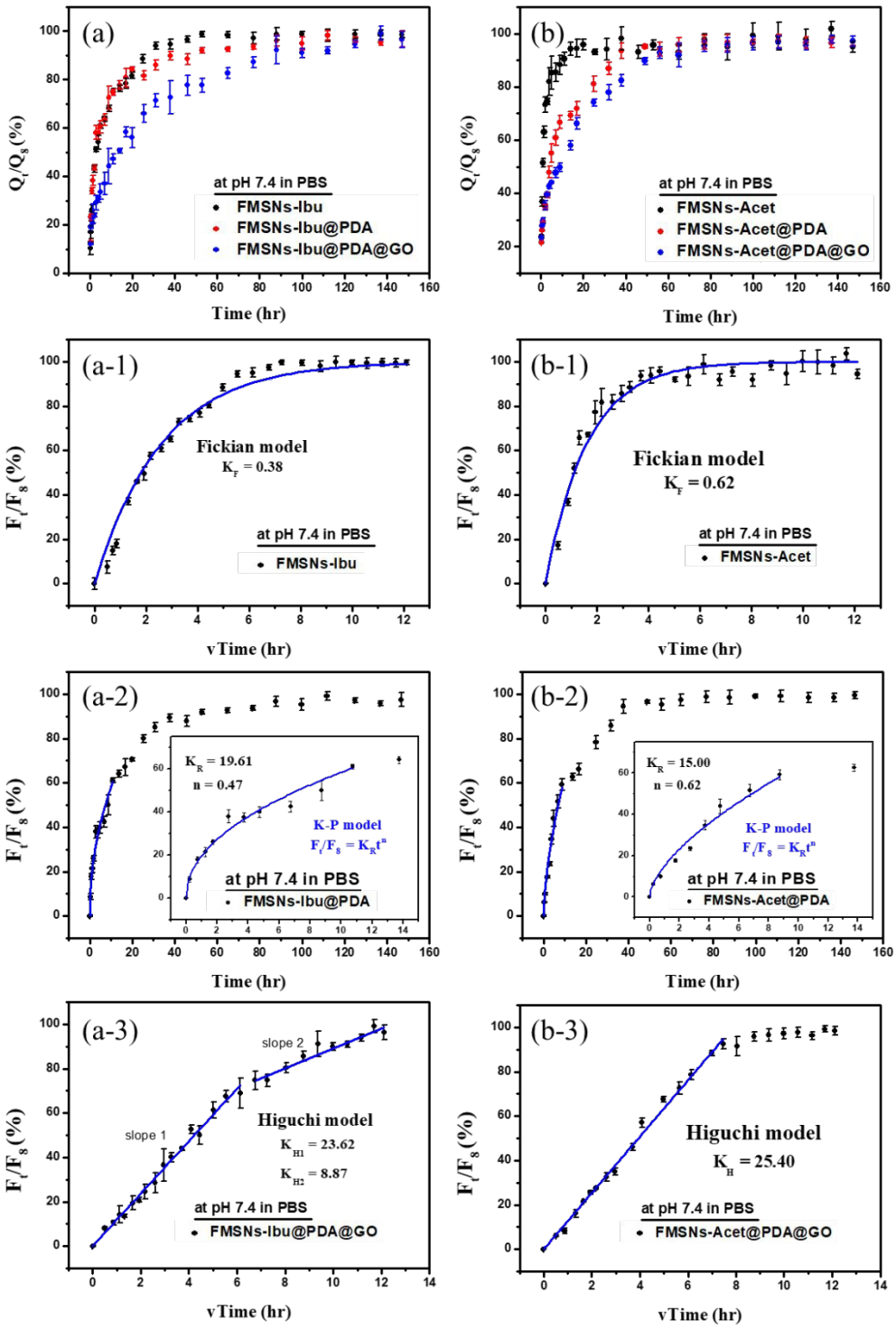

Fig. 5. Release profiles of FMSNs, FMSNs@PDA, and FMSNs@PDA@GO when (a) ibuprofen and (b) acetaminophen were loaded in PBS (pH 7.4) at 37℃. (a, b-1, 2, and 3) Model fits of ibuprofen and acetaminophen release from FMSNs-Drug, FMSNs-Drug@PDA, and FMSNs-Drug@PDA@GO by the Fickian exponential or Higuchi model versus cumulative time or square root time, and K-P model versus cumulative time.

View Article Online
DOI: 10.1039/C9TB02494H

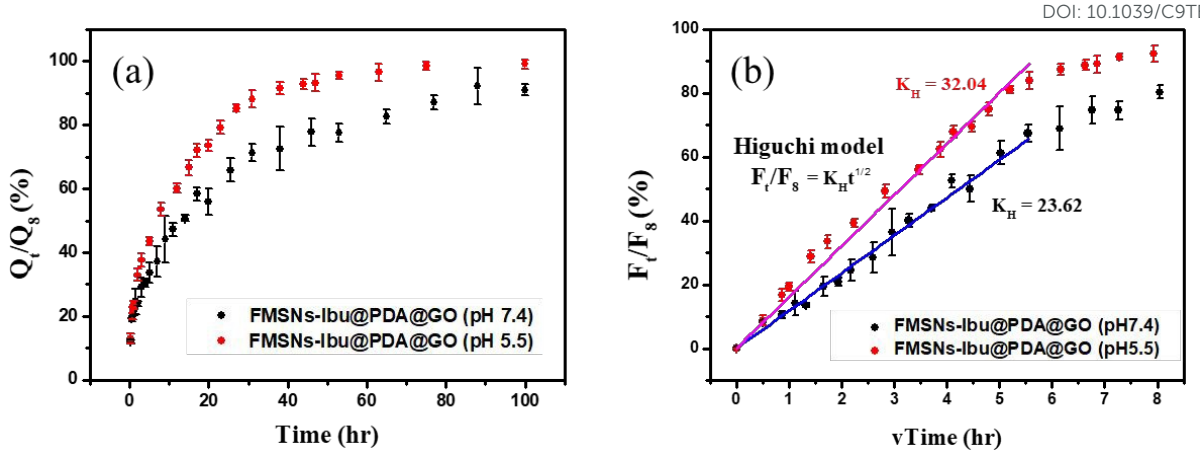

Fig. 6. Release profiles of (a) FMSNs-Ibu@PDA@GO at pH 5.5 and pH 7.4 in PBS. Higuchi model fits of release profiles of (b) FMSNs-Ibu@PDA@GO at pH 5.5 and pH 7.4 in PBS vs square-root-of-time.